

A sensitivity study to global desertification in cold and warm climates: results from the IPSL OAGCM model

Ramdane Alkama · Masa Kageyama ·
Gilles Ramstein

Received: 13 November 2010 / Accepted: 11 May 2011 / Published online: 26 May 2011
© The Author(s) 2011. This article is published with open access at Springerlink.com

Abstract Many simulations have been devoted to study the impact of global desertification on climate, but very few have quantified this impact in very different climate contexts. Here, the climatic impacts of large-scale global desertification in warm (2100 under the SRES A2 scenario forcing), modern and cold (Last Glacial Maximum, 21 thousand years ago) climates are assessed by using the IPSL OAGCM. For each climate, two simulations have been performed, one in which the continents are covered by modern vegetation, the other in which global vegetation is changed to desert i.e. bare soil. The comparison between desert and present vegetation worlds reveals that the prevailing signal in terms of surface energy budget is dominated by the reduction of upward latent heat transfer. Replacing the vegetation by bare soil has similar impacts on surface air temperature South of 20°N in all three climatic contexts, with a warming over tropical forests and a slight cooling over semi-arid and arid areas, and these temperature changes are of the same order of magnitude. North of 20°N, the difference between the temperatures simulated with present day vegetation and in a desert world is mainly due to the change in net radiation related to the modulation of the snow albedo by vegetation, which is obviously absent in the desert world simulations. The enhanced albedo in the desert world simulations induces a large temperature decrease, especially during summer in the cold and modern climatic contexts, whereas the largest

difference occurs during winter in the warm climate. This temperature difference requires a larger heat transport to the northern high latitudes. Part of this heat transport increase is achieved through an intensification of the Atlantic Meridional Overturning Circulation. This intensification reduces the sea-ice extent and causes a warming over the North Atlantic and Arctic oceans in the warm climate context. In contrast, the large cooling North of 20°N in both the modern and cold climate contexts induces an increase in sea-ice extent.

Keywords Desert world · Cold and warm climate · Vegetation-climate feedback · Thermohaline circulation

1 Introduction

Changes in land cover affect global climate via feedbacks between vegetation and the atmosphere. These feedbacks directly modify near-surface energy, moisture, and momentum fluxes via e.g. changes in albedo, leaf area and surface roughness. The presence of vegetation has an impact on the Earth's surface albedo not only through its own albedo, which can contrast with bare soil albedo, but also because high vegetation such as forests can mask snow and therefore limit the increase in albedo related to a recent snowfall. The hydrological cycle is also affected, in many ways, by vegetation, since important variables of this cycle, such as evapotranspiration, is dependent on the plant type. For instance, anthropogenic deforestation in the Tropics during the last few decades is known to have resulted in reduced evaporation, increased surface temperature (e.g. Dickinson and Henderson-Sellers 1988; Lean and Warri- low 1989; Gash et al. 1996; Lean and Rowntree 1997; DeFries et al. 2002; Feddema et al. 2005; Davin and de

R. Alkama (✉)
CNRS/Météo-France, GAME/CNRM, 42 ave. G. Coriolis,
31057 Toulouse, France
e-mail: ramdane.alkama@cnrm.meteo.fr

M. Kageyama · G. Ramstein
LSCE/IPSL UMR CEA-CNRS-UVSQ 8212,
91191 Gif sur Yvette, France

Noblet-Ducoudré 2010), and rising river runoff (Piao et al. 2007).

Studying the impact of changes in vegetation and desertification is therefore relevant for future climate, as it is expected that the increase in global population will significantly alter the use of the Earth's surface in the next centuries (e.g. Ramankutty and Foley 1999; Goldewijk 2001). Furthermore, it has recently been shown that the acceleration of the global warming predicted for the twentyfirst century could induce a die-back of the Amazonian forest as a consequence of reduced precipitation in this region (e.g. Betts et al. 2007). It is also important for our understanding of past climate changes, as the land surface characteristics changed along with climate. For instance, vegetation reconstructions for the last glacial maximum (LGM) show that forests were absent North of 55°N (Bigelow et al. 2003) and tropical forest cover decreased in Asia, Africa, and Australia, whereas the state of the tropical forest in South America is still debated (Harrison and Prentice 2003).

Past studies have investigated the biophysical effects of deforestation in specific modern climatic zones. For example, Henderson-Sellers et al. (1993) showed that deforestation of the Amazonian and South East Asian forests causes temperature reductions over these regions, because of the albedo increase due to deforestation, as well as because of a reduction in local evaporation. They also noted some remote effects of this tropical deforestation such as, for instance, a precipitation increase to the South of the deforested area. Using an AGCM and a scenario in which all tropical rain forests are entirely replaced by grassland, Sud et al. (1996) also found that evapotranspiration decreases but that the outgoing longwave radiation and sensible heat flux increase, which eventually result in a warmer and drier planetary boundary layer. Lean et al. (1997) showed that decreases in roughness associated with deforestation act to reduce evaporation. More recently, Costa and Foley (2000) studied the impact of deforestation in a context of rising atmospheric CO₂ concentration. They found that both deforestation, via the associated decrease in evaporation, and CO₂ increase, via its radiative forcing, tend to increase surface temperature. Finally, Werth and Avissar (2004) demonstrated that a land surface change in a tropical area can cause geopotential surfaces in the upper troposphere to subside, and that these geopotential changes can spread throughout the Tropics and into the midlatitudes. To summarise, the most recent studies about tropical deforestation show that it induces a warming over the deforested area via a decrease in evaporation.

The impact of changes of vegetation in the LGM climate has mainly been studied through sensitivity studies comparing Atmospheric General Circulation Models forced either by a modern (actual or potential vegetation) or a

reconstructed LGM vegetation (Crowley and Baum 1997; Kubatzki and Claussen 1998; Levis et al. 1999; Wyputta and McAvaney 2001; Harrison and Prentice 2003; Ramstein et al. 2007). These studies have therefore not focused on as large a change as global deforestation and climate differences related to these two different vegetation covers appear to be of second order, but not negligible, compared to the impact of other changes in boundary conditions relevant for the LGM, i. e. northern hemisphere ice-sheets and decrease in atmospheric CO₂ concentrations. However, vegetation changes can be important regionally. Indeed, using HadSM3 coupled to the dynamical vegetation model TRIFFID to simulate LGM climate, Crucifix and Hewitt (2005) demonstrated that over Eurasia, particularly over Siberia and the Tibetan plateau, the response of the biosphere substantially enhances the glacial cooling through a positive feedback loop between vegetation, temperature, and snow-cover. They also find that in central Africa, the decrease in tree fraction results in a reduction in precipitation. The atmosphere dynamics, and more specifically the Asian summer monsoon system, are significantly altered by remote changes in vegetation: the coolings in Siberia and Tibet act in concert to shift the summer subtropical front southwards and to weaken the easterly tropical jet and the associated momentum transport. Thus, climatic changes related to the use of a more realistic vegetation cover in LGM climate simulations can be regionally important and suggest that changes in vegetation should be taken into account for detailed model-data comparisons. However, the LGM vegetation is not well known everywhere, which makes the assessment of the impact of LGM vegetation difficult. Here, by choosing an idealised set-up, i.e. global desertification, we aim at examining the impact of one of the largest possible changes in surface characteristics.

Fraedrich et al. (1999) and Kleidon et al. (2000) use an AGCM with modern boundary conditions and study the impact of a “green” and a “desert” world. They find that a desert world is associated with a less intense hydrological cycle, and that surface temperatures are generally higher due to decreased evapotranspiration. They noted, however, that this sensitivity could be dependent on the climatic context. Furthermore, oceanic feedbacks were missing in all of above studies. One study of the atmosphere–ocean response to changes in vegetation is that of Renssen et al. (2003), who showed that large-scale changes in preindustrial forest cover may lead to a non-linear response of the ocean thermohaline circulation. They analyzed the transient response of the atmosphere–ocean system to a deforestation and showed that the initial cooling due to the albedo decrease is further amplified by sea ice formation at high latitudes in a first step, and in a second step to a southward shift of the North Atlantic convection sites, which further acts to cool the northern hemisphere high

latitudes by decreasing the North Atlantic northward heat transport. This then feeds back on the sea-ice cover and high latitude temperatures, which cool enough to induce year-round snow cover over North America and northern Scandinavia.

In the case of preindustrial climate it is clear that there is an important feedback between the vegetation and the thermohaline circulation (Renssen et al. 2003) but this feedback could be negligible for other climatic contexts, especially as far as the slowdown of the thermohaline circulation is concerned. On the one hand, in the case of a warmer world, there is some speculation that a shutdown or a slowdown of the thermohaline circulation could occur, via a warmer North Atlantic and Arctic sea surface temperatures (IPCC 2007). On the other hand, for the LGM, the deep water formation in the North Atlantic was shown to be less intense than today (Duplessy et al. 1980; Boyle and Keigwin 1987) and the Atlantic meridional overturning circulation cell to be limited in the vertical (McManus et al. 2004; Piotrowski et al. 2005; Lynch-Stieglitz et al. 2007). Here we will study whether these first order responses in AMOC could be modified by vegetation changes.

Our study investigates the combined ocean–atmosphere response to large-scale land surface change in cold (LGM), modern and warm climates (with an atmospheric CO₂ concentrations equal to 185, 280 and 836 ppm, respectively), using the IPSL_CM4 OAGCM. In the present study, we only consider the biogeophysical effects of vegetation. Therefore, this study completes the studies of Fraedrich et al. (1999) and Renssen et al. (2003), by performing the same type of desert world experiments with a fully coupled AOGCM and for different climatic contexts. Our aim is to use the same series of experiments in three different climatic contexts to investigate how the same perturbation, i.e. global desertification, may lead to different responses, depending on the background climate. It is therefore an ideal set-up to investigate the following three issues:

1. What are the impacts of vegetation on the atmospheric energy balance?
2. What are the impacts of global desertification on the hydrological cycle?
3. What are its consequences for the ocean dynamics?

Finally we aim at analyzing the similarities and differences on a large spectrum of climatic conditions.

2 Methodology

We have performed numerical experiments using the IPSL_CM4 coupled ocean–atmosphere–sea-ice general

circulation model (Marti et al. 2010). The atmospheric model LMDz (Hourdin et al. 2006) and the land-surface model ORCHIDEE (Krinner et al. 2005) are run with a horizontal resolution of 96 points in longitude, 72 points in latitude ($3.75^\circ \times 2.5^\circ$) and 19 vertical levels for the atmosphere. The ocean component, ORCA/OPA (Madec et al. 1998) is run with 182 points in longitude, 149 points in latitude and 31 vertical levels with the highest resolution (10 m) in the upper 150 m, the horizontal mesh is curvilinear and orthogonal on the sphere, the grid spacing is about 2° , with a refined resolution of $\sim 0.5^\circ$ near the Equator. The sea-ice model LIM2 (Fichefet and Morales Maqueda 1997), which computes ice thermodynamics and dynamics, is included in the ocean–atmosphere model. The models are coupled using the OASIS coupler (Valcke et al. 2004), which interpolates the net surface heat flux, the net water flux, solar flux, and the wind stresses from the atmosphere model grid to the ocean model grid, and the SST and the sea-ice cover from the ocean model grid to the atmosphere model grid. The models exchange the time-averaged files once a day.

We define three series of two model experiments (Table 1). In the first series, labeled CS for “control simulation”, the present-day vegetation cover is imposed in the ORCHIDEE land-surface model. The LAI seasonal cycle is prescribed following the mean observed LAI seasonal cycle (Loveland et al. 2000), repeated during the whole simulation. In the second series, labeled DW for “desert world”, vegetation is replaced by bare soil. In these simulations, the surface albedo is initially the same as the CS bare soil albedo, but during the run, the albedo can be modified by different moisture or snow cover.

The first two simulations are denoted FUT (FUT for “postulated future with present day vegetation”) and FUTd (the subscript d referring to desert world). In those simulations we use the modern topography and orbital parameters, and greenhouse gases fixed at the 2100 values of the SRES A2 scenarios. We use the same boundary conditions, except for modern atmospheric greenhouse gas concentrations, in the MOD and MODd (referring to modern simulations, prescribing present day vegetation in the first simulation and a desert world in the second simulation). These simulations are denominated as “modern” simulations because they use modern vegetation, coastlines and ice sheets. However, greenhouse gases are fixed at their preindustrial values. In the last two simulations, LGMR (R referring to Realistic LGM river as explained in Alkama et al. 2006 and 2008) and LGMRd, we use the LGM boundary conditions: ice sheets and coastlines according to Peltier (2004) (ICE-5G), LGM greenhouse gases and orbital parameters, following the PMIP2 recommendations (<http://pmip2.lsce.ipsl.fr>, Braconnot et al. 2007). The present day vegetation is used in the LGMR experiment

Table 1 Summary of the boundary conditions used for the numerical experiments analyzed in the present study

Experiment	Vegetation	Albedo computation based on	CO ₂ (ppm)	CH ₄ (ppb)	N ₂ O (ppb)	Ice sheets	Orbital parameters
FUT	Present	Vegetation	836	3731	477	Modern	Present (2000)
FUTd	Desert world	Bare soil					
MOD	Present	Include Vegetation	280	790	270	Modern	Present (2000)
MODd	Desert world	Bare soil					
LGMR	Present	Vegetation	185	350	200	ICE-5G	21ky BP
LGMRd	Desert world	Bare soil					

(as recommended by PMIP2) and deserts are prescribed in the LGMRd simulation. The annual mean LAI and LGM ice sheets margins which are used in this study are shown on Fig. 1 and Table 1. Our “Desert World” experiments are therefore sensitivity experiments which we compare to existing simulations run for the IPCC AR4 or PMIP2. The LGMR run was itself initiated from another LGM run and is at equilibrium for ocean meridional overturning circulation, global surface temperature or global bottom ocean temperatures. This LGMR simulation is 1,000 years long and these parameters are stable after the first 150 years. The DW sensitivity run has been started from year 350 of the CS LGM run. The MOD run has also been run for 1,000 years. The DW simulation is started from year 600 of the CS simulation. The FUT simulation starts at the end of the SRES A2 IPCC simulation, which itself started from the MOD run. It is therefore not in total equilibrium with the imposed greenhouse gases, as for all simulations of this type. The FUTd simulation starts with the same initial conditions. Each DW run consists in a 150-year-long numerical integration of which the last 20 years are analyzed, compared to the corresponding 20 years of the associated CS run. At this stage, the first order response to global desertification is reached, for example, in terms of global continental and oceans surface temperature.

Even though we have used pre-industrial greenhouse gas concentrations in our MOD simulation, we can compare its results to the observed modern global hydrological cycle, since there are only small differences in global precipitation, runoff and evaporation over the twentieth century (Dai et al. 1997; Milliman et al. 2008; Alkama et al. 2011). The model simulates the modern global hydrological cycle satisfactorily compared to observations (Trenberth et al. 2007) (see Table 2 and Fig. 2). In none of our simulations we have taken into account the flood plains and evaporation from reservoirs, marshes and lakes. This can explain the difference in the evaporation over the continents E_c ; and consequently on the continental precipitation P_c , between the simulated values and the observations. From this brief study and the available analyses on other aspects of the simulated atmosphere and ocean states (cf. Marti et al. 2010), we conclude that the model’s representation of the global hydrological cycle is satisfactory enough to use this tool to determine its sensitivity to extreme climatic contexts (cold and warm) and extremes of vegetation cover (present-day vegetation vs. desert world). The scope of this section is not to evaluate the IPSL_CM4 model in detail (see Marti et al. 2010, for a detailed review of the model’s performances) but rather to show that the temperature and the hydrological cycle are simulated with enough accuracy to be used for our series of experiments.

Fig. 1 Annual mean leaf area index (m^2/m^2) of present day vegetation used in this study. The blue contour represents the LGM ice sheets limit. Antarctica has been omitted

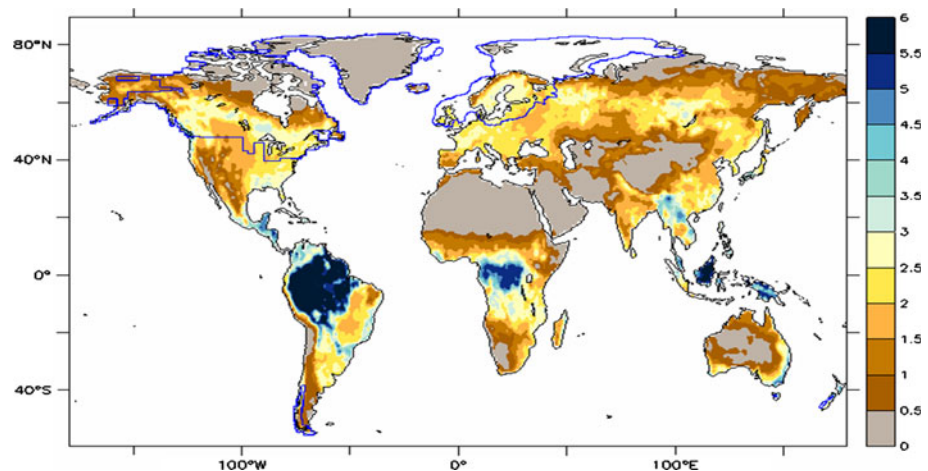


Table 2 Modern experiment versus data

	Temp (°C)	Eo (mm/year)	Po (mm/year)	Ec (mm/year)	Pc (mm/year)	R (mm/year)
Trenberth et al. (2007)	14	1178	1064	495	766	271
MOD experiment	14	1170	1067	420	664	244

Comparison of the hydrological cycle and temperature simulated by the IPSL_CM4 model in the MOD simulation to the data (Trenberth et al. 2007). The notations are explained in Fig. 2

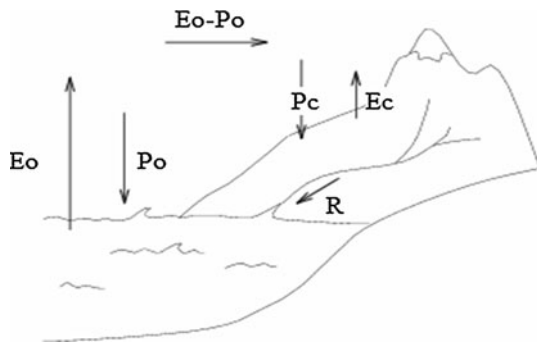


Fig. 2 Hydrological cycle notations for the global cycle. E_o Evaporation over the ocean, P_o Precipitation over the ocean, E_c and P_c Evaporation and precipitation over the continents, R Runoff

3 Results: sensitivity to global desertification in cold and warm climates

In this section, we discuss the results of the six experiments (DW vs. CS in the three climatic contexts), focusing on the global energy and water balance (issues 1 and 2), and on the dominant atmospheric and ocean circulation patterns (issue 3).

3.1 Global water and energy balance

Figure 3a gives the global and annual averages of the temperature, surface and top of the atmosphere energy fluxes for the desert world (DW, top row of each table of 3×3 numbers), control simulations (CS which use present day vegetation, middle row) and their differences (DW–CS, bottom row) for the warm (in red), modern (in black) and cold (in blue) climates. All energy flux values are normalized w.r.t the incoming solar radiation. First, we examine the anomaly fields globally averaged over the continents. The shortwave radiation absorbed at the surface decreases by 3, 7 and 9% in DW w.r.t. CS in the warm, modern and cold climates respectively. The most important changes in the surface energy budgets are the 63, 64 and 61% reductions in upward latent heat transfers in the warm, modern and LGM climates, respectively. This is consistent with previous studies (e.g. Fraedrich et al. 1999).

Along with the changes in latent heat transfer, the upward shortwave anomalies at the surface 20, 34, 33% (for the warm, modern and LGM climates, respectively)

appear to be related to the increased albedo anomalies (11, 31 and 30%). The values of the differences for the outgoing short wave radiation and the albedo do not exactly correspond to each other because of differences in incoming short wave fluxes. These differences are due to the influence of changes in the atmospheric water vapor and cloudiness which are reduced by about 42, 19 and 17%. Along with a reduction in evaporation in the DW experiments and a colder ground temperature (from 0.2 to 3.2°C), the upward longwave radiation decreases, as well as the downward longwave radiation. Because of the reductions of the atmospheric water content, the total continental longwave radiation budget at the surface tends to cool the DW climate, as does the shortwave budget, but with a smaller magnitude in both modern and cold climates. In contrast, the future warm climate, in which the difference in the atmospheric water vapor is maximum (42%, while it does not exceed 20% in both of the present and LGM climates), the long wave effect on the surface land temperature becomes larger than the short wave effect.

For all climatic contexts, a desert world results in hydrological cycle weakening: precipitation, evaporation and atmospheric moisture all decrease, except for the runoff which increases (Fig. 3b). The land evapotranspiration (E_c) decreases by about 49, 50 and 51% in the warm, modern and LGM climates respectively. This induces a $\sim 25\%$ decrease in land precipitation in all three climatic contexts. Consequently, the runoff is increased about 9, 11 and 15% in the warm, modern and cold climate respectively. This amplification is larger in the low atmospheric CO_2 case (cold climate), probably due to a stronger stomatal conductance effect (Gedney et al. 2006; Betts et al. 2007; Alkama et al. 2010). Indeed, for a low atmospheric CO_2 , plants' stomata open more or longer to absorb the CO_2 they need for their growth but this adaptation of the stomata to lower CO_2 conditions also results in a larger transpiration of water than for higher CO_2 . This therefore acts to reduce runoff in the CS simulations, and the reduction is larger for lower atmospheric CO_2 values. In the DW simulations, this effect is not active anymore, so, compared to the CS runs, the runoff is larger, and the increase is larger for lower values of CO_2 .

Finally, global desertification also affects the hydrological cycle over the oceans. The evaporation over the ocean (E_o) decreases by about 4% in all runs. This contributes to a decrease in precipitation over the oceans,

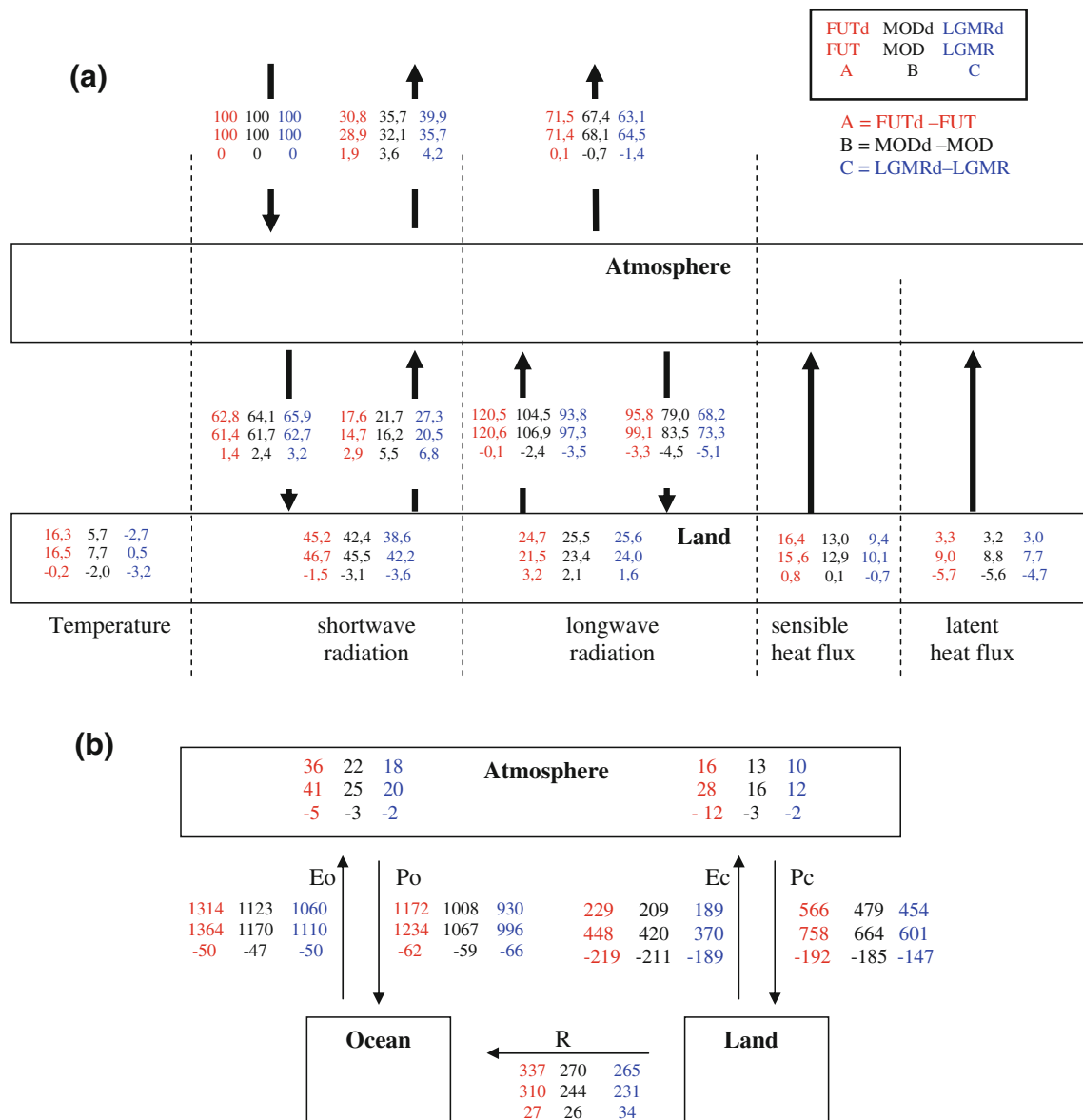


Fig. 3 Annual mean of (a) the surface energy balance over land (all figures normalised by incoming TOA SW radiation); (b) the global water cycle: annual mean water fluxes in mm/year and precipitable water in kg/m², and heat/radiative fluxes in percent incoming

radiation (100% = 341,3 W/m²) for the desert world (*upper*), present day vegetation (*middle*), and desert world minus present day vegetation. Future simulation in red, modern in black and LGM in blue

largest for the LGM (7%) compared to the modern (6%) and warm (5%) climates. More details concerning the ocean heat and hydrological budgets and their consequences on modifying ocean circulation are given in Sect. 3.3.

3.2 Spatial patterns in the response to desertification

3.2.1 Temperature

Figure 4 shows the mean annual temperature anomalies between the CS and DW experiments. In general, South of 20°N, the patterns of the temperature anomalies are the

same in the three different contexts. The largest anomalies (DW–CS) are positive and located over tropical forest regions, where they can reach up to 7°C. Elsewhere, they are much smaller and the oceans are slightly cooler. The largest temperature increase over the Tropics in all three climate contexts occurs in summer due to the reduced latent heat flux caused by the absence of vegetation. Between 20 and 40°N, the land surface temperature anomalies between DW and CS in the cold and modern climates appear to have roughly the same magnitude. The intensity of this cooling increases rapidly northward, over the boreal forest regions, with maximum values of 15 and

18°C in the Modern and LGM climates respectively, maxima which are located around the latitude of 65°N. The temperature response to desertification is therefore especially strong in the regions where the difference in the albedo is at its largest (Fig. 5). This large albedo difference occurs especially in the northern north hemisphere due to differences in snow albedo being masked by vegetation in CS, but not in DW (Fig. 6). This maximum corresponds to the maximum boreal forest density. In these regions the temperature anomaly can exceed 20°C in the modern and cold climates, especially in summer when the snow is largely melted in the CS simulation compared to the DW experiment. Over the ocean, the largest temperature decrease in the modern and cold DW experiments is due to a larger sea ice extent. The small temperature increase located at 50°N over the Atlantic is due to an intensified Atlantic Meridional Overturning Circulation (AMOC) in the DW simulation which is associated with an increased northward heat transport (for more details on the AMOC changes and associated differences in sea-ice extent, see Sect. 3.3).

The smaller temperature anomalies in the warm climate case (Fig. 4a) is due to less extensive snow-covered regions in the CS runs (Fig. 6). In this climate too, the AMOC is more intense in DW compared to CS experiments. As a result, more heat is transported from the equator into the Arctic via the Atlantic Ocean. This induces large sea-ice free areas over the Arctic Ocean and consequently a warming over this region (Fig. 7). Also, in this warm context, contrary to what occurs in the modern and cold climates, the largest temperature decrease occurs in winter, due to the albedo and snow cover differences occurring in this season, whereas the simulated temperatures are less different in summer.

3.2.2 Precipitation

The response to global desertification in terms of precipitation (Fig. 8a–c) clearly shows a drier atmosphere, especially over the continents. This signal corresponds to a reduced evaporation from the surface in the DW simulations (Fig. 8d–f). The anomalies are minor over desert areas, the maxima are located over tropical forest areas. Except for the Tibetan plateau and Amazonia (and Congo in MOD and LGM climates), the decrease in continental evaporation is larger than the decrease in continental precipitation (Fig. 8g–i). This explains the increased runoff in DW runs (Fig. 3b).

The $P-E$ response to global desertification over the North Atlantic is negative North of 40°N. This feature is essentially due to an increase in evaporation since precipitation is mostly unchanged. This negative $P-E$ acts to increase the AMOC, which in turn modifies the

$P-E$ pattern: when the AMOC strengthens, it brings warmer waters northward, as depicted on Figs. 9 and 4 which show that the cooling is less strong over the North Atlantic ocean than over the adjacent continents for both the cold and modern climate, and that there is even warming in some areas, which acts to enhance evaporation. There are therefore contrasting mechanisms for the evolution of the AMOC: increased runoff on the one hand, increased evaporation over the convection sites of the North Atlantic on the other. The next section further examines the consequences of global deforestation on the ocean dynamics.

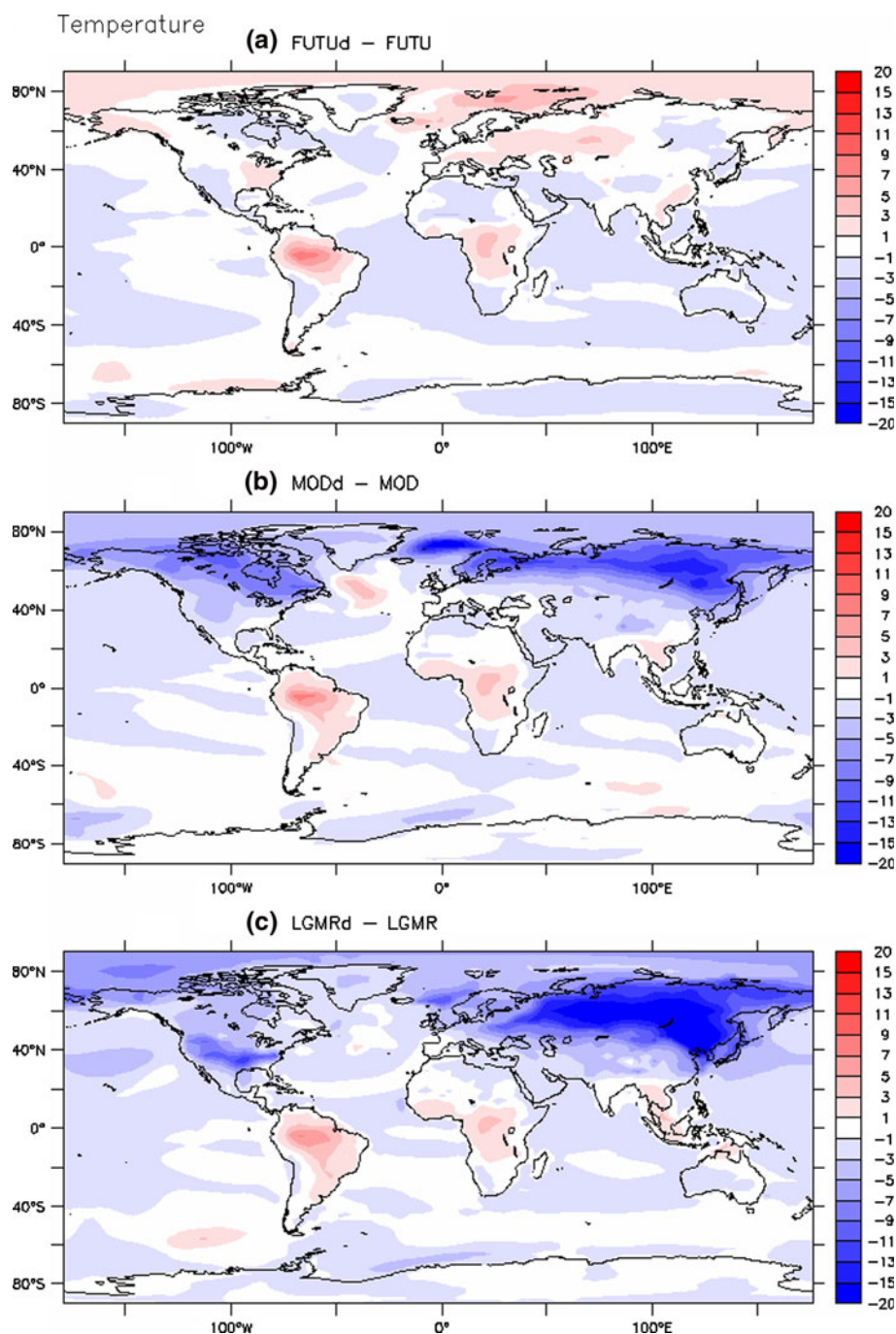
3.3 Ocean circulation and feedback

The AMOC is sensitive to the salinity and temperature over convections sites of the Labrador, Irminger and Greenland Iceland Norwegian (GIN) Seas. Previously, we have seen that the temperature and hydrological cycles are largely impacted by global desertification. Here, we quantify the fresh water input into the convection sites in order to investigate the factors controlling the AMOC via changes in salinity. The total fresh water input into the northern North Atlantic, GIN Seas and Arctic Oceans is the sum of the runoff of the rivers, calving from the ice-sheets and atmosphere to ocean fluxes (precipitation–evaporation). In our model, this ‘calving’ term is, in fact, in the absence of a coupling to an ice sheet model, the snow that falls in excess of the threshold of 3,000 kg/m² over the ice sheets and which is redistributed over the oceans to close the freshwater budget in the model, to prevent a salinity drift. There is little change in this calving term between the DW and CS simulations. The decrease of total freshwater flux to the oceans (about 20,000 m³/s for LGM, 33,000 m³/s for modern, and 42,000 m³/s for future climates) in the DW simulation compared to CS is in fact mainly due to the decrease in the atmosphere to ocean freshwater flux (Table 3).

This drying of the North Atlantic and Nordic Seas should favour an intensification of the AMOC. Indeed, the DW simulations produce an increase in the meridional overturning cell. This increase in intensity and in the cell’s vertical size is larger in the cold climates with a maximum of 12 Sv (1 Sv = 10⁶ m³/s) in the LGM and modern climates, while it is only about 3 Sv in the warm climate. The North Atlantic overturning maximum anomaly is located at 500, 2000, 2,500 m in the warm, modern and LGM climates, respectively (Fig. 9).

From the fact that the AMOC increases for the warm climate, even though the sea surface temperature over the Arctic and North Atlantic increases, we conclude that the AMOC anomalies are largely related to the freshwater change over these areas and that temperature changes play a second role and cannot counterbalance the increase in

Fig. 4 Annual means temperature anomaly **a** FUTd-FUT, **b** MODd-MOD and finally **c** LGMRd-LGMR

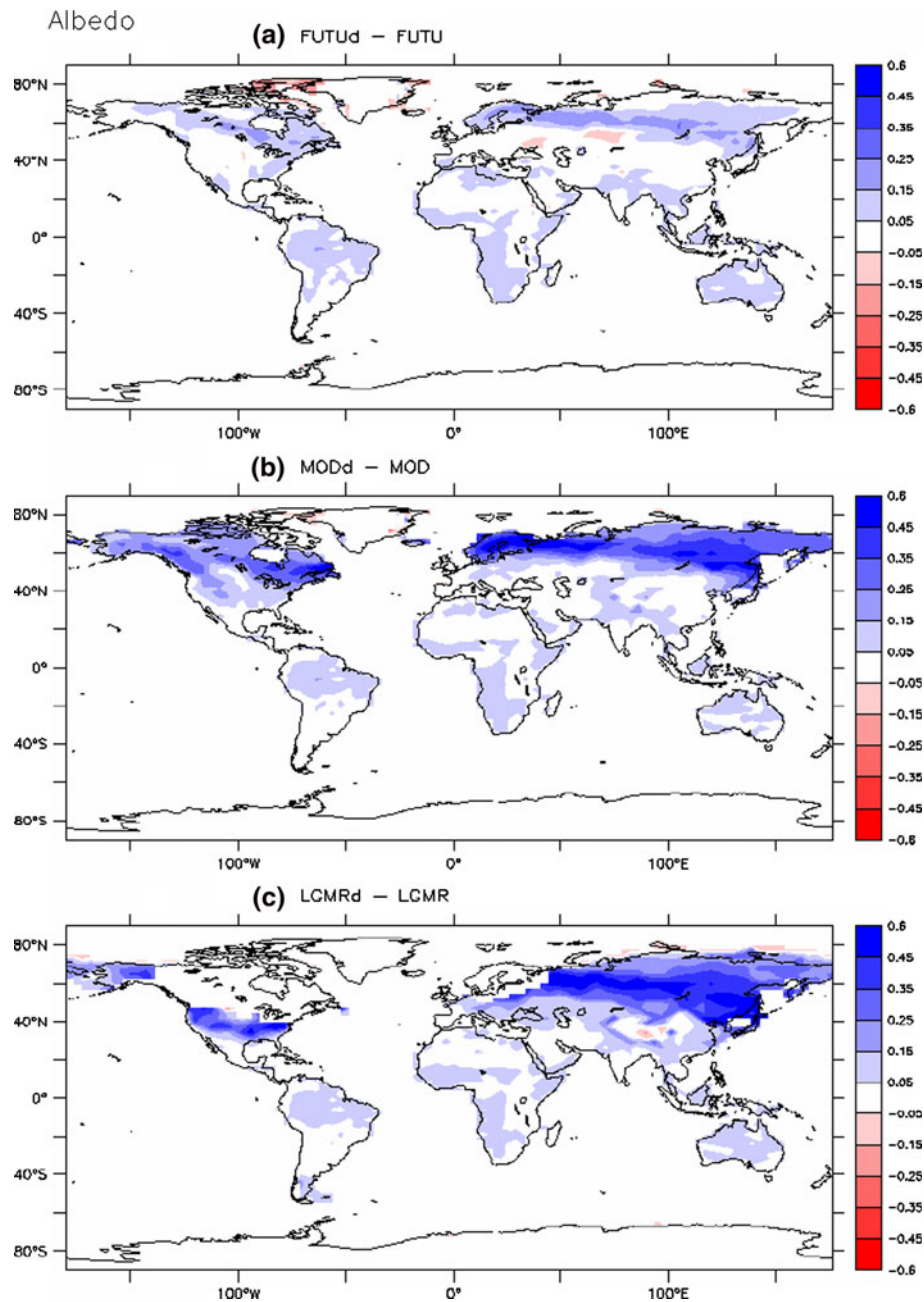


salinity in the warm climate case. In contrast, the northern high latitude cooling in the DW simulations for both the modern and cold climates favours Arctic sea-ice formation, and consequently more saline waters North of 80°N (Fig. 10). Along with colder temperatures in the North Atlantic and the Arctic (Fig. 11), this can explain the intensified North Atlantic Deep Water formation in the DW experiments. The AMOC smaller strengthening in the warm context can be explained by the fact that in this case, the AMOC is initially less intense and the fact that the

temperature effect counterbalances the reduction of fresh-water over the Arctic and North Atlantic, as is the case in many simulations under increased greenhouse gas concentrations (IPCC 2007).

The intensification of the AMOC in DW compared to CS induces a strengthening in oceanic heat transport. Figure 12 shows that the global meridional oceanic heat transport is amplified by more than 0.15 PW when averaged between 10°S and 60°N in all climatic contexts. In the case of the warm and modern climates, this increase is

Fig. 5 Annual mean anomaly in surface albedo **a** FUTd-FUT, **b** MODd-MOD and finally **c** LGMd-LGMR

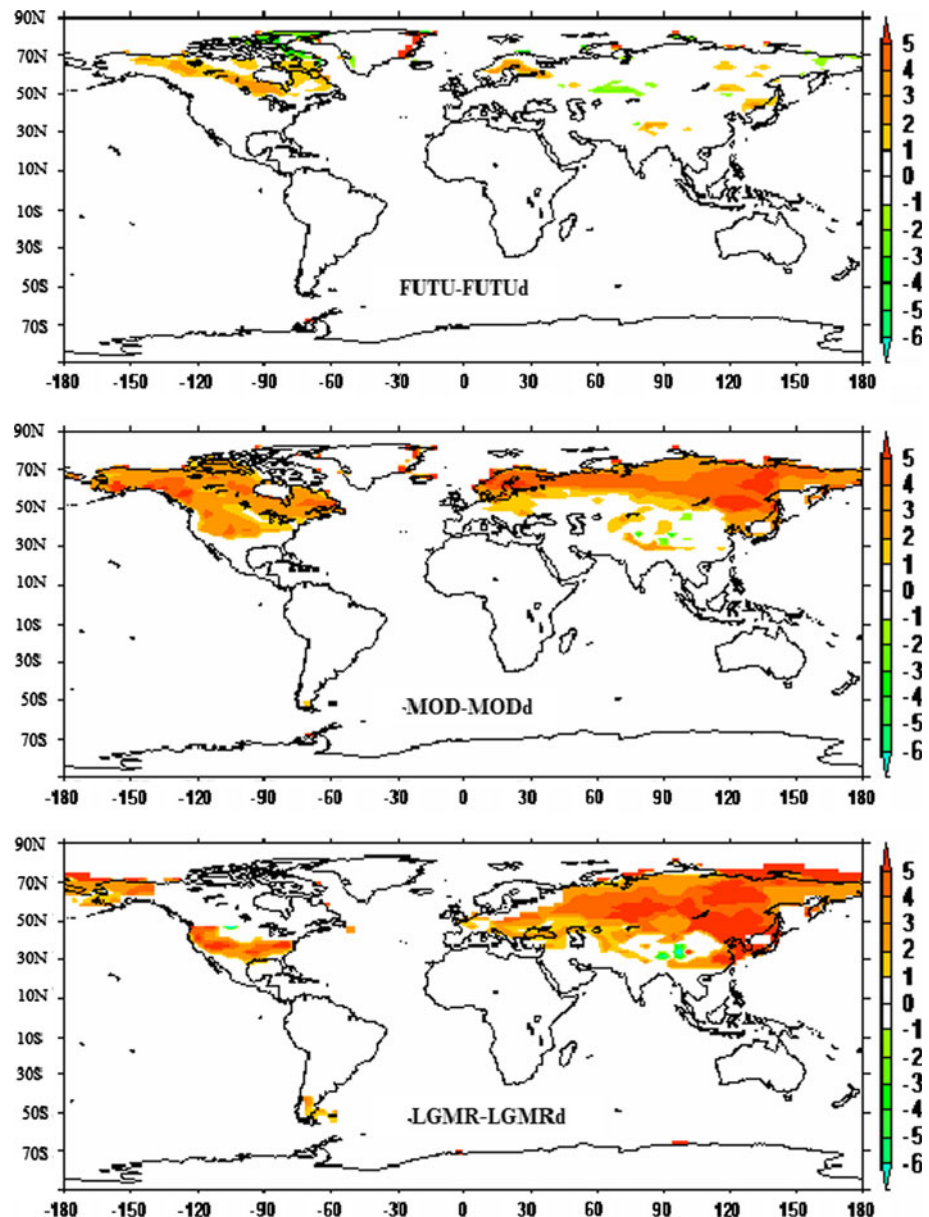


mainly explained by the amplification of the Atlantic meridional heat transport, related to the intensification of the AMOC. Indeed, for these climatic contexts, the Atlantic explains more than 80% of the difference in total difference oceanic meridional heat transport. Alternatively, for the LGM climate, the Atlantic ocean is only responsible for less than 50% of the global oceanic meridional heat transport difference. At higher latitudes (60°N–90°N), the oceanic northward meridional heat transport is amplified by about 0.1 PW in the warm climate. This increase is mainly explained by the reduction of the sea-ice extent in DW compared to CS (Fig. 7 left column). In contrast, for

the same latitudes, the increase of the Atlantic and Arctic sea-ice extent in both the modern and cold DW climates (Fig. 7 middle and right column) induces a reduction of oceanic northward meridional heat transport but of smaller magnitude (about 0.05 PW in the modern and only about 0.01 PW in the LGM climate).

The upper panel of Fig. 12 shows that the atmospheric meridional heat transport decreases in response to the increase in oceanic meridional heat transport in the case of the warm climate. This type of effect has been depicted by Bjerknes (1964) and is therefore usually called the “Bjerknes compensation” effect (Shaffrey and Sutton,

Fig. 6 Anomalies in the number of months with snow cover: FUTd–FUT (*upper*), MODd–MOD (*middle*) and LGMRd–LGMR (*bottom*)



2006). In order to have a perfect compensation, a constant radiative budget and no storage in any heat reservoirs are required. Even though these hypotheses are not verified here, we see that the atmospheric heat transport compensation seems to be total. This suggests that the increased albedo over continents (Siberia) via increasing snow cover is compensated by the decline of sea ice extent. In the case of the modern and cold climates (Fig. 12, middle and bottom panels), the Bjerknes compensation is far from being satisfied, showing that the climate system has largely modified its radiative budget and heat storage in response to the changes in the AMOC. These modifications in radiative budget are notably due to changes in sea-ice cover that modifies the albedo and therefore the radiative budget (Winton 2003) and to continental albedo change related to

snow cover. In these climatic contexts, the difference in the radiative budget between the DW and CS is large enough to prevent the compensation between the anomalies in oceanic and atmospheric heat transports.

4 Summary and discussion

In this work, we evaluate the climatic impacts of a global desertification using the IPSL_CM4 OAGCM in cold (LGM), modern and warm climates (2100 SRES A2 conditions). Two numerical runs have been performed for each climate. One simulation uses the present day vegetation whereas the second uses a desert world forcing, defined as a world in which the continental surface is only bare soil,

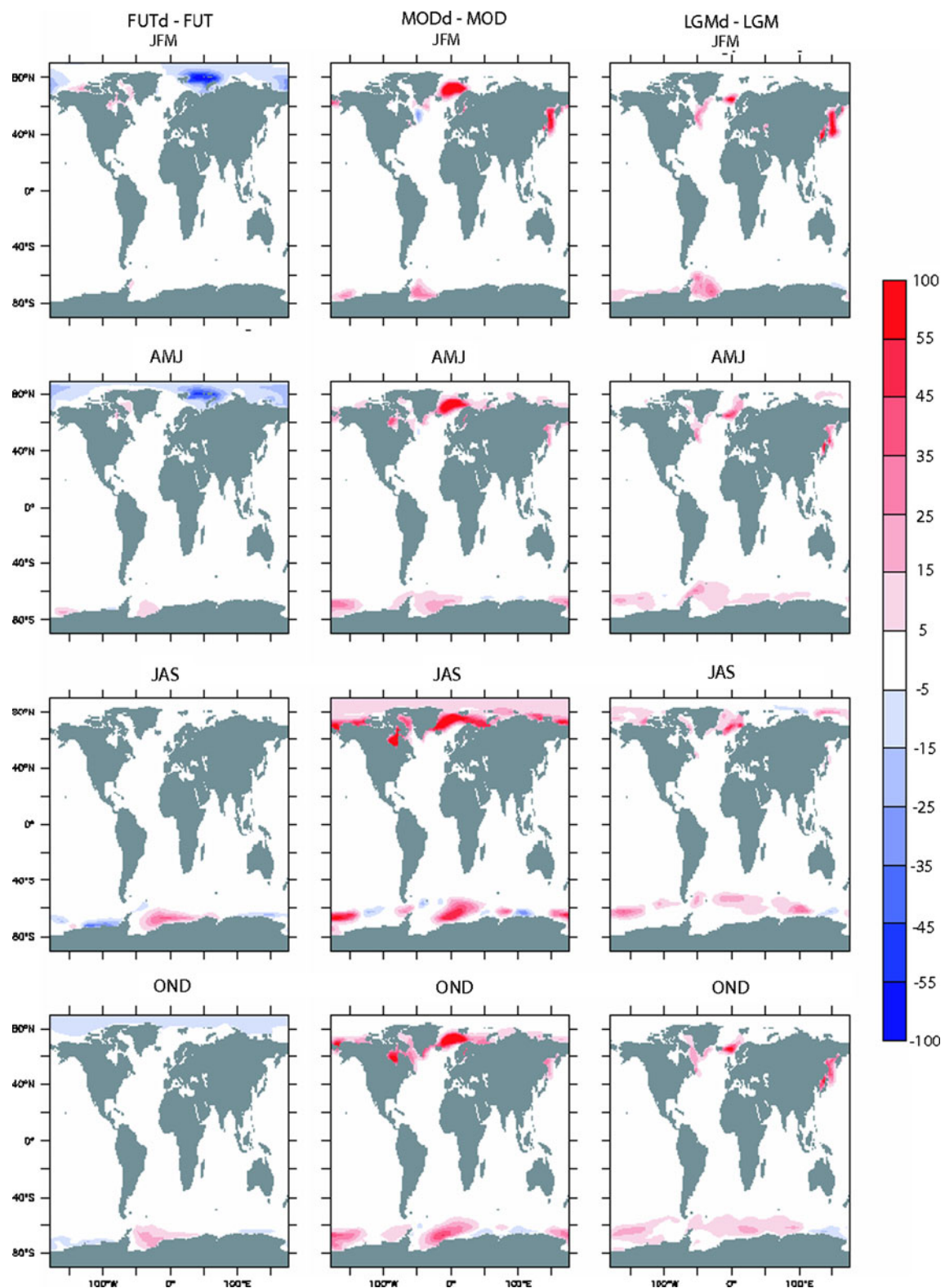


Fig. 7 Seasonal anomalies in percentage of the sea ice cover: FUTd-FUT (left), MODd-MOD (middle) and LGMRd-LGMR (right column)

and this bare soil has the same characteristics as the bare soil in the reference simulation. One limitation of this study consists in the duration of the DW simulations, which is

only 150 years while 800 years would be needed to equilibrate the deep ocean (Renssen et al. 2003). However, the processes observed in our simulations, such as

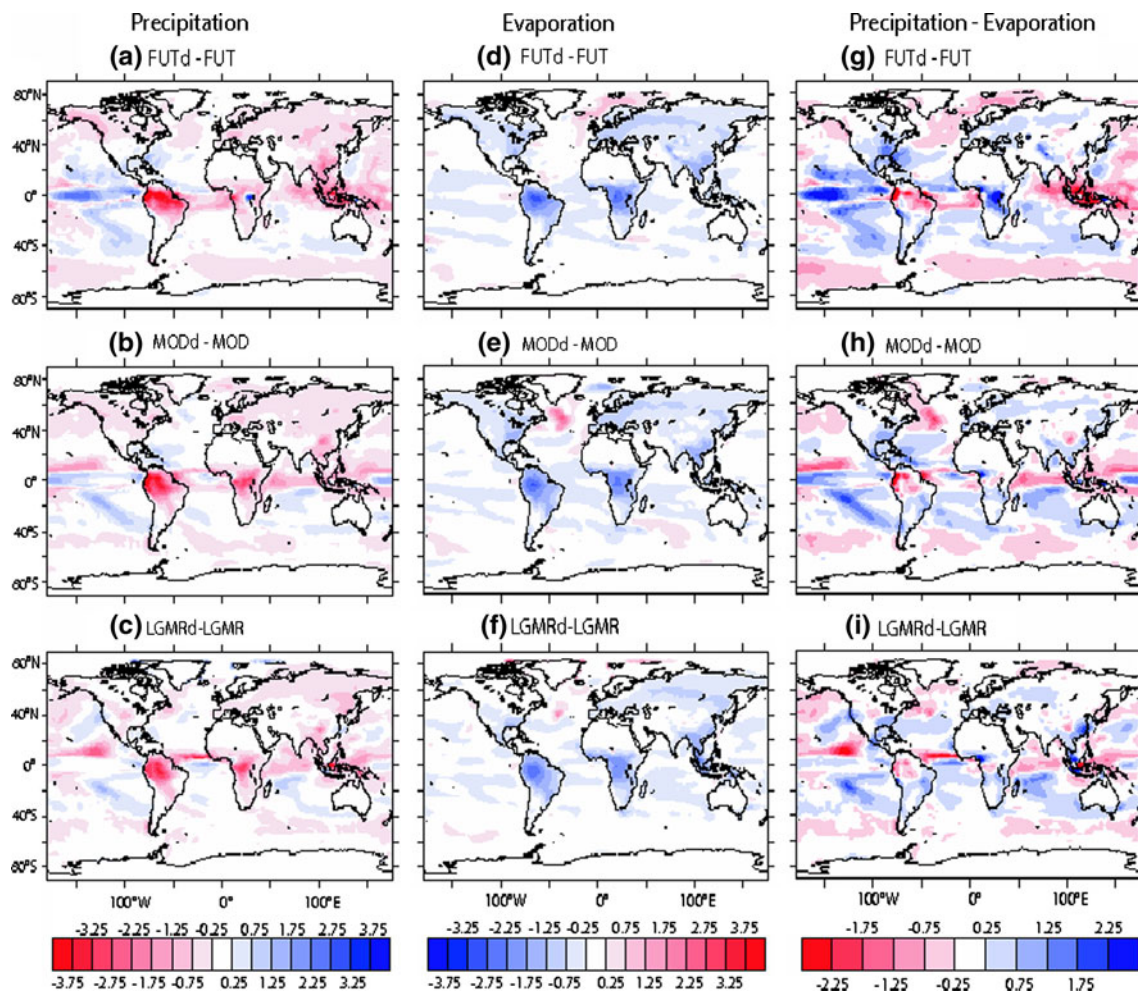


Fig. 8 Annual mean anomaly in precipitation, evaporation and precipitation minus evaporation (mm/day) (a, d, g) FUTd-FUT, (b, e, h) MODd-MOD and finally (c, f, i) LGMRd-LGMR

modifications of the atmospheric energy budget, surface temperature and even sea-ice extent changes are actually relatively fast. In the first order, the equilibrium is reached after 70 years in both modern and LGM simulations, where 90 years are needed to equilibrate the future climate. This can not exclude a possible long term change due to an abrupt change in depth ocean circulation. However, we did not see such adjustments in all millenniums IPSL-CMIP5 experiments. After the analysis of the six simulations designed to investigate the sensitivity to global desertification in three climate contexts, we can bring answers to the three issues raised in the introduction.

1. What are the impacts of vegetation on the energy balance of the three different climatic states?

As demonstrated previously by Fraedrich et al. (1999) and Kleidon et al. (2000), our study confirms that the main impact of removing the vegetation on the energy budget is

the large reduction in upward latent heat transfer. This reduction is of the same order of magnitude for the three climate contexts over tropical forest areas. In semi-arid and arid areas, the effect of the absence of vegetation in DW is mainly seen through changes in energy balance related to the cloud response. Indeed, the reduction of cloud cover in DW induces a reduction of the downward longwave radiation resulting in a slight cooling. In the case of modern and cold climates, the dominant signal in terms of the temperature change North of 20°N is related to changes in net surface radiation related to increase in albedo in DW. This has already been noticed in previous massive deforestation studies (e.g. Betts 2001; Bounoua et al. 2002; Davin and de Noblet-Ducoudré 2010). This increase is due to the fact that in the DW runs, the snow is not masked by vegetation as it is in CS. Indeed, the temperature response to desertification is especially strong in the boreal regions where forests are present in CS. Consequently, the upward shortwave flux increases at the surface and induces a large

Fig. 9 Anomalies in the Atlantic Ocean stream function between DW and CS. The values South of 30°S represent the global stream function values. The contour interval is 1 Sv. *R* yellow and red shading denotes positive values; green and blue negative values

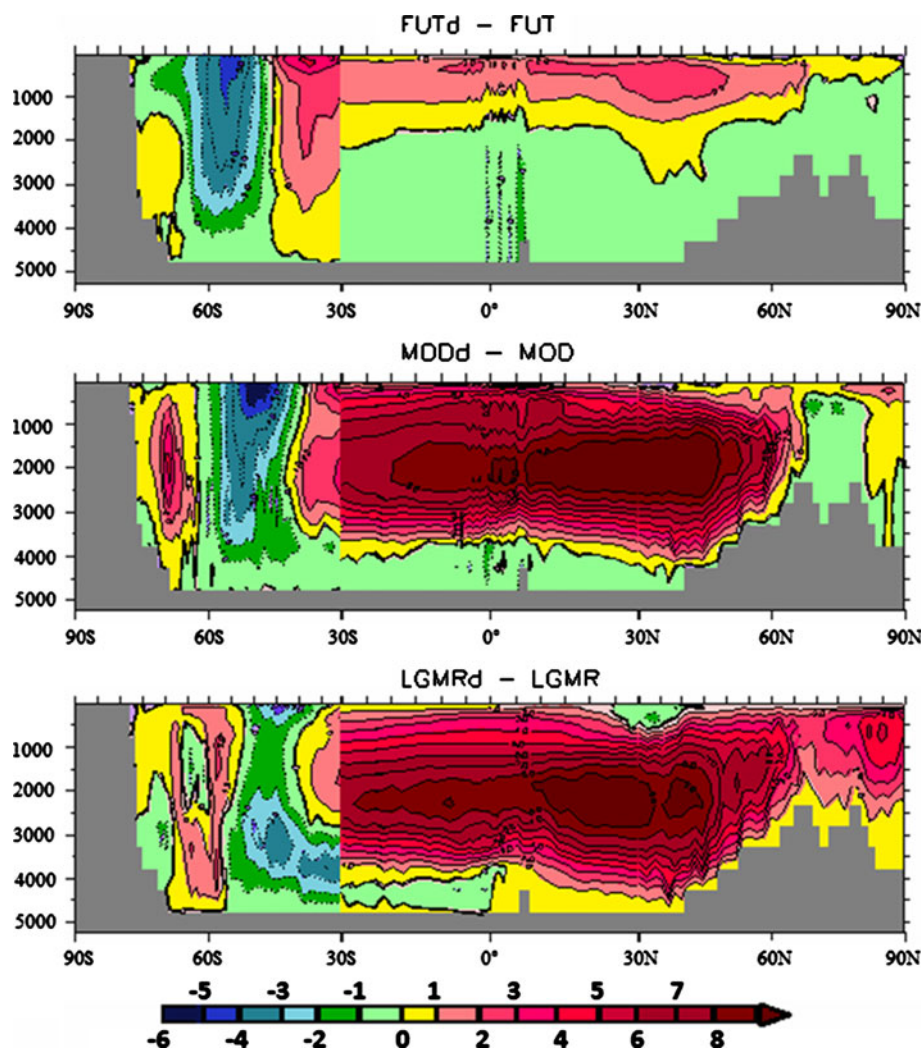


Table 3 Freshwater input over Atlantic and Arctic oceans 45–90°N in different simulations

	FUT	FUTd	A	MOD	MODd	B	LGMR	LGMRd	C
River flow (1,000 m ³ /s)	482	509	27	338	355	17	158	173	15
Calving (1,000 m ³ /s)	23	22	−1	19	16	−3	163	154	−9
Atmosphere to ocean (1,000 m ³ /s)	355	287	−68	235	188	−47	129	103	−26
Total freshwater (1,000 m ³ /s)	860	818	−42	592	559	−33	450	430	−20
Maximum AMOC (Sv)	3	6	3	12	20	8	12	21	9

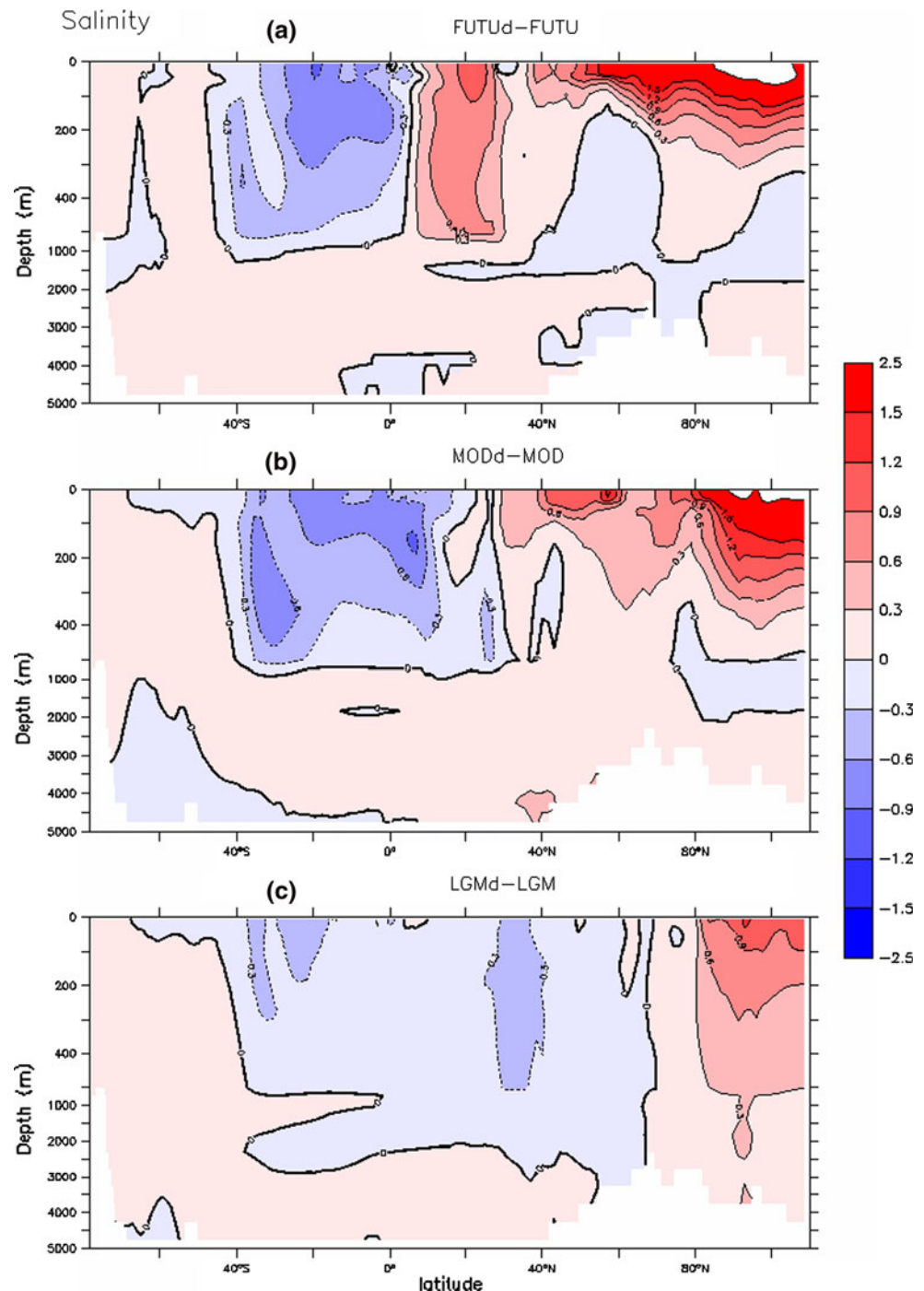
$A = \text{FUTd} - \text{FUT}$, $B = \text{MODd} - \text{MOD}$ and $C = \text{LGMRd} - \text{LGMR}$

cooling. Here we show that, in the case of a warm climate, this cooling occurs only during the winter. In the other seasons, the net impact of desertification is a slight warming because the reduction in latent heat flux and in surface roughness are responsible for the dominant impacts in these regions.

2. What are the impacts of global desertification on the hydrological cycle?

One of the direct consequences of the reduction of the latent heat transfer (evaporation) and cooling in the desert world is the reduction of the atmospheric water vapor and clouds. This results in decreasing precipitation. In short, global desertification results in a hydrological cycle weakening. This confirms the previous findings by Fraedrich et al. (1999). An exception to this general weakening is the slight increase in runoff. As described before, this increase is larger in the cold (LGM) than in the warm and

Fig. 10 Atlantic latitude-depth sections salinity **a** FUTd–FUT **b** MODd–MOD and **c** LGMRd–LGMR



modern climates, probably due to the stomatal conductance effect. Indeed, less CO_2 in the atmosphere acts to intensify the evapotranspiration in the LGM CS simulation because plants regulate the opening and closing of their stomata in response to changing environmental conditions: in a low- CO_2 atmosphere, their stomata open more or for longer, and more water is lost from leaves to the atmosphere (Field et al. 1995). As a consequence, plants can acquire enough carbon through their stomata

but with more water uptake from the soil. The result is that continental evapotranspiration is amplified (Betts et al. 1997), less moisture is left in the soil, and this can lead to decreased continental runoff (Gedney et al. 2006). Because of the presence of the plants, global evapotranspiration is greater in CS compared to DW runs. This difference is amplified in LGM because of the lower atmospheric CO_2 level, resulting in a largest runoff increase due to vegetation (CS vs. DW simulations),

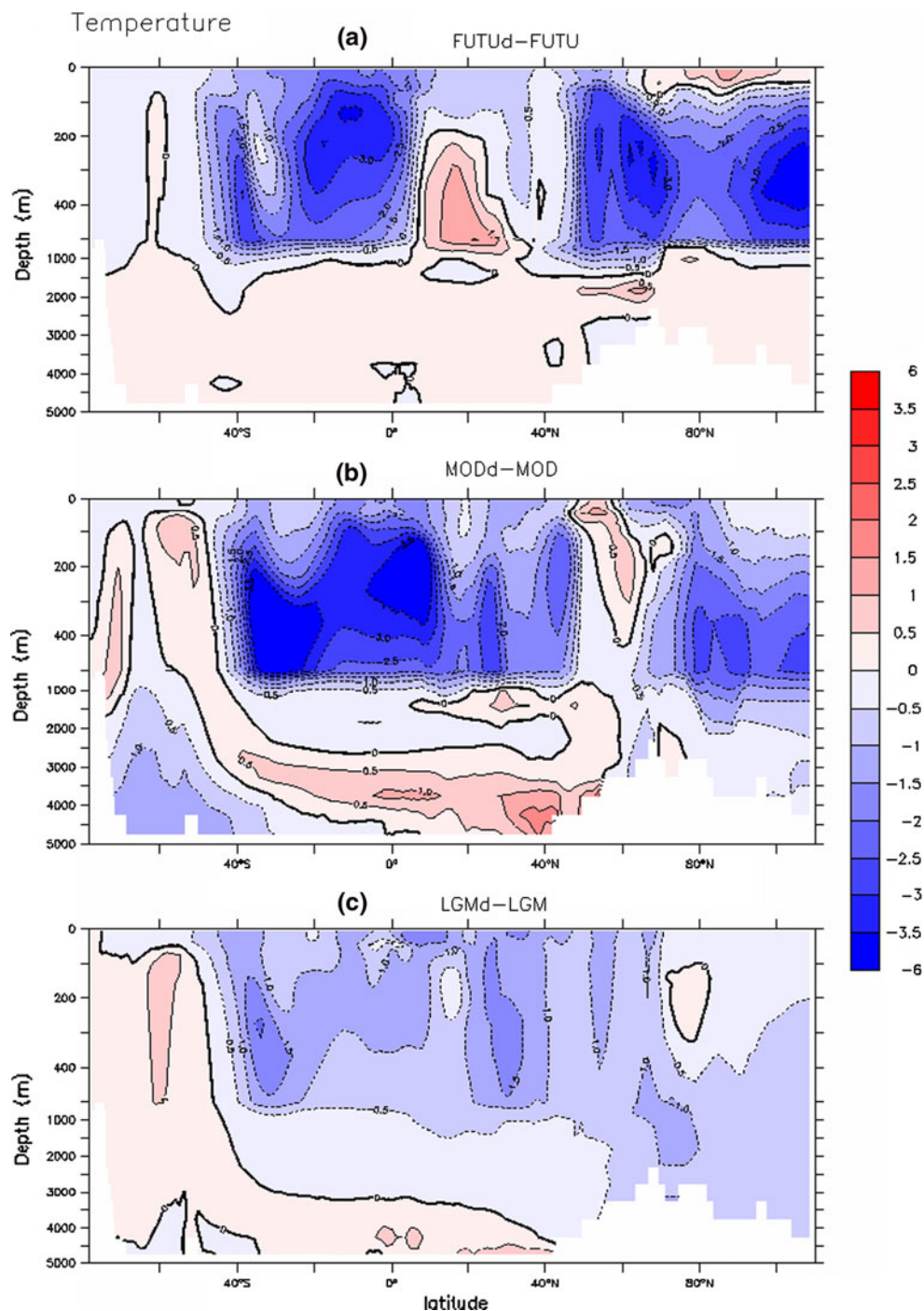


Fig. 11 Atlantic latitude-depth sections temperature **a** FUTd-FUT **b** MODd-MOD and **c** LGMd-LGM

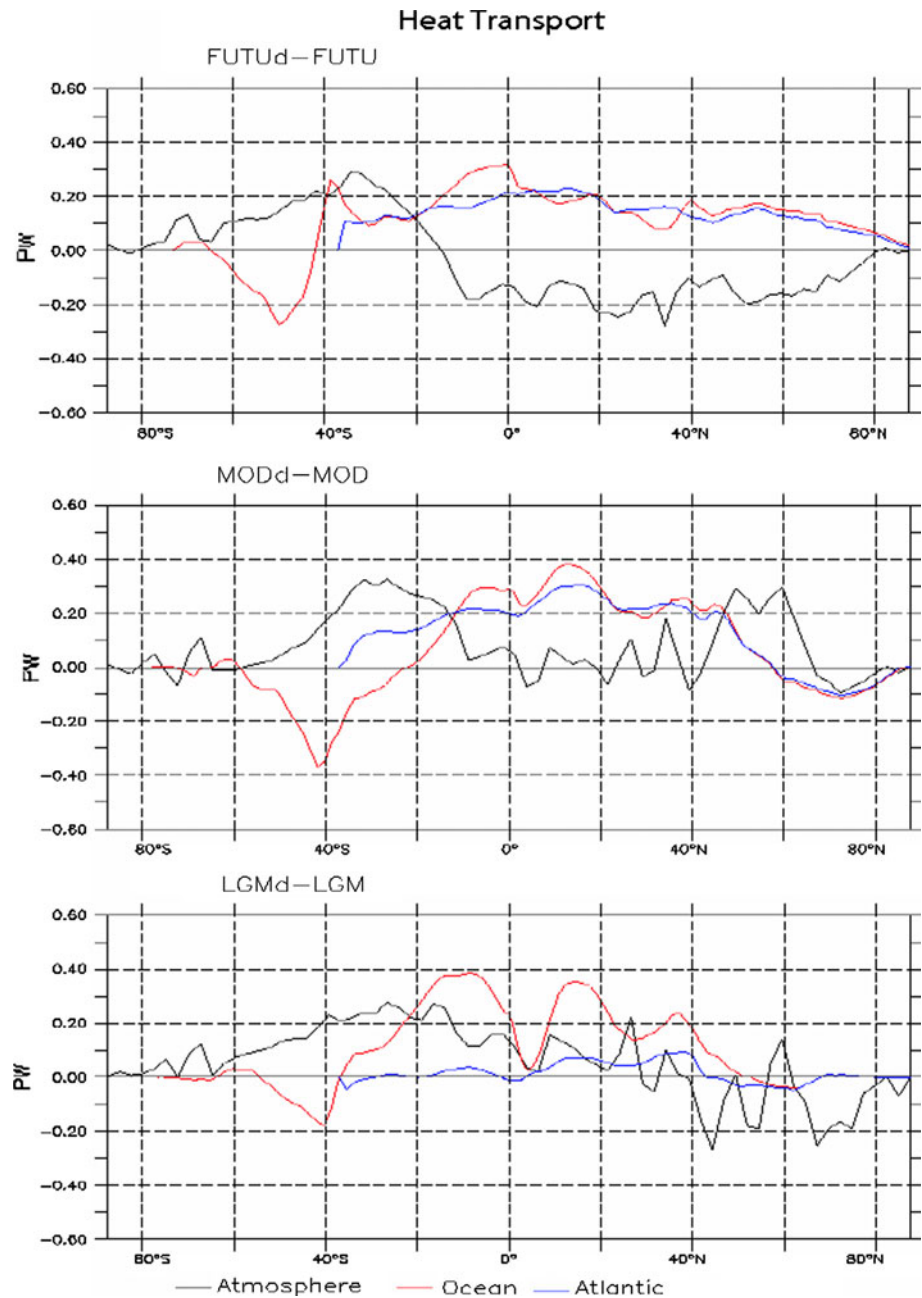
compared to the warm and modern climates. In the present study, the CO_2 fertilization effect is not taken into account. As shown by Piao et al. (2007) and Gerten et al. (2008) an increase in the leaf area index due to a higher atmospheric CO_2 level can induce an increase in the transpiration and consequently contribute to decreasing river runoff, therefore compensating the response due to changes in evapotranspiration. Additional simulations,

with interactive LAI, would be needed to assess the CO_2 fertilization effect in the three climatic contexts studied here.

3. What are the consequences for the ocean dynamics?

This study also highlights the importance of the coupling with the ocean. Up to now, most of our knowledge concerning the impact of land cover change on climate

Fig. 12 Difference in zonally averaged meridional heat transport (PW) between the FUTUd and FUTU (*upper*), MODd and MOD (*middle*), and LGMd and LGM (*bottom*) simulations. In *red* is the oceanic heat transport difference, in *black* the atmospheric heat transport difference and in *blue* the Atlantic heat transport difference



came from atmospheric-only models, assuming fixed oceanic conditions (e.g. Nobre et al. 1991; Fraedrich et al. 1999; Kleidon et al. 2000; Gedney and Valdes 2000; Chase et al. 2000; Voldoire 2006). Implicitly, this assumption was justified by the fact that the perturbation owing to land cover change is applied to the land and not to the ocean. However, our experiments show that taking the coupling with the ocean into account greatly affects the simulated response to desertification. First, as demonstrated by Renssen et al. (2003), we noted that the ocean surface responds to desertification by a cooling. But this cooling is not generalised and differs from one climate to another, especially over North Atlantic and Arctic. In the case of the

modern and cold climate contexts, the more extensive sea-ice formation in the Arctic and/or North Atlantic due to the cooler temperatures at high latitudes induces an amplification of the AMOC and a southward shift of the convective sites in which the temperature slightly increases compared to CS runs. In all other surrounding regions, temperature decrease, especially over the regions where new sea ice appears. To compensate this large cooling over regions North of 40°N, both the oceanic and atmospheric meridional heat transports increase. In contrast, in the warm climate, the increased AMOC is largely due to the increased salinity over the Arctic and North Atlantic. This intensification of the AMOC induces an important

strengthening in northward oceanic heat transport that is counterbalanced by the reduction of the meridional atmospheric heat transport.

Finally, does vegetation have a different impact for a warm, a modern and a cold climate context?

Supporting earlier hypothesis which studied the impact of deforestation (e.g. Pielke et al. 2002; Davin et al. 2007), we showed that desertification triggers two contrasting mechanisms: a radiative one (owing to surface albedo change) and a non radiative one (owing to change in evapotranspiration efficiency and roughness). We found that, replacing the vegetation by bare soil has roughly similar impacts South of 20°N in all three climatic contexts. This impact is mainly dominated by the non radiative forcing. In the other hand, the main differences concern the latitudes North of 20°N, where the snow cover and sea-ice extent play an important role in modifying the albedo and consequently the ocean and atmosphere dynamics. In both the modern and cold climatic contexts in which there is snow, global desertification causes an increase in albedo which enhances the upward shortwave radiation and thus cause a cooling (via radiative forcing). There is less snow in the warm climate compared to the modern and cold ones. Indeed, continental snow cover is only simulated in winter in the future climate runs, with a larger extent and albedo in DW compared to the CS warm climate. As consequence, North 20°N, in the future DW run, the seasonal cycle is more contrasted, with cooler winters and warmer springs, summers and autumns, especially over areas where there are forests in the corresponding control run. This warming is principally caused by the reduction in latent heat flux (i. e. non radiative forcing) and in the sea-ice extent. This sea ice extent decrease is due to an increase of the evaporation over the North Atlantic and the Arctic which acts to enhance the salinity (density) and consequently the AMOC, resulting to an intensification of oceanic northward heat transport.

Acknowledgments This work has been supported by ANR-BLANC IDEGLACE and the RTRA STAE Toulouse, with computer time provided by CEA/CCRT. The authors wish to thank the three anonymous reviewers for their useful comments on this paper.

Open Access This article is distributed under the terms of the Creative Commons Attribution Noncommercial License which permits any noncommercial use, distribution, and reproduction in any medium, provided the original author(s) and source are credited.

References

- Alkama R, Kageyama M, Ramstein G (2006) Freshwater discharges in a simulation of the last glacial maximum climate using improved river routing. *Geophys Res Lett* 33:L21709. doi: [10.1029/2006GL027746](https://doi.org/10.1029/2006GL027746)
- Alkama R, Kageyama M, Ramstein G, Marti O, Ribstein P, Swengedouw D (2008) Impact of a realistic river routing in coupled ocean-atmosphere simulations of the last glacial maximum climate. *Clim Dyn* 30:855–859
- Alkama R, Kageyama K, Ramstein G (2010) Relative contributions of climate change, stomatal closure and leaf area index changes to 20th and 21st century runoff change: a modelling approach using the ORCHIDEE land surface model. *J Geophys Res* 115:D17112. doi: [10.1029/2009JD013408](https://doi.org/10.1029/2009JD013408)
- Alkama R, Decharme B, Douville H, Ribes A (2011) Trends in global and basin-scale runoff over the late 20th century: methodological issues and sources of uncertainty. *J Clim* doi: [10.1175/2010JCLI3921.1](https://doi.org/10.1175/2010JCLI3921.1)
- Betts RA (2001) Biogeophysical impacts of land use on present-day climate: near-surface temperature change and radiative forcing. *Atmos Sci Lett* 2:39–51. doi: [10.1006/asle.2001.0037](https://doi.org/10.1006/asle.2001.0037)
- Betts RA et al (1997) Contrasting physiological and structural vegetation feedbacks in climate change simulations. *Nature* 387:796–799
- Betts RA, Boucher O, Collins M, Cox PM, Falloon PD, Gedney N, Hemming DL, Huntingford C, Jones CD, Sexton DM, Webb MJ (2007) Links projected increase in continental runoff due to plant responses to increasing carbon dioxide. *Nature* 30:448(7157): 1037–1041
- Bigelow NH, Brubaker LB, Edwards ME et al (2003) Climate change and Arctic ecosystems: 1. Vegetation changes north of 55 degrees N between the last glacial maximum, mid-holocene, and present. *J Geophys Res* 108:11–1–11–25
- Bjerknes J (1964) Atlantic air–sea interaction. *Adv Geophys* 10:1–82
- Bounoua L, DeFries R, Collatz GJ, Sellers P, Khan H (2002) Effects of land cover conversion on surface climate. *Clim Change* 52:29–64
- Boyle EA, Keigwin LD (1987) North Atlantic thermohaline circulation during the past 20000 years linked to height latitude surface temperature. *Nature* 330:35–40
- Braconnot P, Otto-Bliesner B, Harrison S, Joussaume S, Peterchmitt J-Y, Abe-Ouchi A, Crucifix M, Driesschaert E, Fichefet Th, Hewitt CD, Kageyama M, Kitoh A, Laîné A, Loutre M-F, Marti O, Merkel U, Ramstein G, Valdes P, Weber SL, Yu Y, Zhao Y (2007) Results of PMIP2 coupled simulations of the mid-holocene and last glacial maximum—part 1: experiments and large-scale features. *Clim Past* 3:261–277. doi: [10.5194/cp-3-261-2007](https://doi.org/10.5194/cp-3-261-2007)
- Chase TN, Pielke RA, Kittel TGF, Nemani RR, Running SW (2000) Simulated impacts of historical land cover changes on global climate in northern winter. *Clim Dyn* 16:93–105
- Costa MH, Foley JA (2000) Combined effects of deforestation and doubled atmospheric CO₂ concentrations on the climate of Amazonia. *J Clim* 13:18–34
- Crowley TJ, Baum SK (1997) Effect of vegetation on an ice-age climate model simulation. *J Geophys Res* 102(D14):16463–16480
- Crucifix M, Hewitt CD (2005) Impact of vegetation changes on the dynamics of the atmosphere at the last glacial maximum. *Clim Dyn* 25(5):447–459. doi: [10.1007/s00382-005-0013-8](https://doi.org/10.1007/s00382-005-0013-8)
- Dai A, Fung IY, Del Genio AD (1997) Surface observed global land precipitation variations during 1900–1988. *J Clim* 10:2943–2962
- Davin EL, de Noblet-Ducoudré N (2010) Climatic impact of global-scale deforestation: radiative versus nonradiative processes. *J Clim* 23(1):97–112
- Davin EL, de Noblet-Ducoudré N, Friedlingstein P (2007) Impact of land cover change on surface climate: relevance of the radiative forcing concept. *Geophys Res Lett* 34:L13702. doi: [10.1029/2007GL029678](https://doi.org/10.1029/2007GL029678)
- DeFries RS, Bounoua L, Collatz GJ (2002) Human modification of the landscape and surface climate in the next fifty years. *Glob Change Biol* 8:438–458

- Dickinson RE, Henderson-Sellers A (1988) Modelling tropical deforestation: a study of GCM land-surface parameterizations. *Q J R Meteorol Soc* 114:439–462
- Duplessy JC, Moyes J, Pujol C (1980) Deep water formation in the North Atlantic Ocean during the last ice age. *Nature* 286:479–482
- Feddema J, Oleson K, Bonan G, Mearns L, Buja LE, Meehl GA, Washington WM (2005) The importance of land-cover change in simulating future climates. *Science* 310:1674–1678
- Fichefet T, Morales Maqueda MA (1997) Sensitivity of a global sea ice model to the treatment of ice thermodynamics and dynamics. *J Geophys Res* 102:12609–12646
- Field C, Jackson R, Mooney H (1995) Stomatal responses to increased CO₂: implications from the plant to the global scale. *Plant Cell Environ* 18:1214–1255
- Fraedrich K, Kleidon A, Lunkeit F (1999) A green planet versus a desert world: estimating the effect of vegetation extremes on the atmosphere. *J Clim* 12(10):3156–3163
- Gash JHC, Nobre CA, Roberts JM, Victoria RL (1996) Amazonian deforestation and climate. Wiley, Chichester, p 595
- Gedney N, Valdes PJ (2000) The effect of Amazonian deforestation on the Northern Hemisphere circulation and climate. *Geophys Res Lett* 27:3053–3056
- Gedney N, Cox PM, Betts RA, Boucher O, Huntingford C, Stott PA (2006) Detection of a direct carbon dioxide effect in continental river runoff records. *Nature* 439(7078):835–838
- Gerten D, Rost S, von Bloh W, Lucht W (2008) Causes of change in 20th century global river discharge. *Geophys Res Lett* 35:L20405. doi:[1029/2008GL035258](https://doi.org/10.1029/2008GL035258)
- Goldewijk KK (2001) Estimating global land use change over the past 300 years: the HYDE database. *Glob Biogeochem Cycles* 15(2):417–433
- Harrison SP, Prentice AI (2003) Climate and CO₂ controls on global vegetation distribution at the last glacial maximum: analysis based on palaeovegetation data, biome modelling and palaeoclimate simulations. *Glob Change Biol* 9(7):983–1004
- Henderson-Sellers A, Dickinson RE, Durbidge TB, Kennedy PJ, McGuffie K, Pittman AJ (1993) Tropical deforestation: modeling local- to regional-scale climate change. *J Geophys Res* 98:7289–7315
- Hourdin F, Musat I, Bony S, Braconnot P, Codron F, Dufresne JL, Fairhead L, Filiberti MA, Friedlingstein P, Grandpeix JY, Krinner G, Levan P, Li ZX, Lott F (2006) The lmdz4 general circulation model: climate performance and sensitivity to parametrized physics with emphasis on tropical convection. *Clim Dyn* 27(7–8):787–813
- IPCC (2007) Climate change 2007: the physical science basis. In: Solomon S, Qin D, Manning M, Chen Z, Marquis M, Averyt KB, Tignor M, Miller HL (eds) Contribution of working group I to the fourth assessment report of the intergovernmental panel on climate change. Cambridge University Press, Cambridge
- Kleidon A, Fraedrich K, Heimann M (2000) A green planet versus a desert world: estimating the maximum effect of vegetation on land surface climate. *Clim Change* 44:471–493
- Krinner G, Viovy N, de Noblet-Ducoudré N, Ogée J, Polcher J, Friedlingstein P, Ciais P, Sitch S, Prentice IC (2005) A dynamic global vegetation model for studies of the coupled atmosphere-biosphere system. *Glob Biogeochem Cycles* 19:1015–1029
- Kubatzki C, Claussen M (1998) Simulation of the global biogeophysical interactions during the last glacial maximum. *Clim Dyn* 14(7–8):461–471
- Lean J, Rowntree PR (1997) Understanding the sensitivity of a GCM simulation of Amazonian deforestation to the specification of vegetation and soil characteristics. *J Clim* 10:1216–1235
- Lean J, Warrilow DA (1989) Simulation of the regional climatic impact of Amazon deforestation. *Nature* 342:411–413
- Lean J, Button CB, Nobre C, Rowntree PR (1997) The simulated impact of Amazonian deforestation on climate using measured ABRACOS vegetation characteristics. In: Gash JHC, Nobre C, Roberts JM, Victoria RL (eds) Amazonian deforestation and climate. Wiley, Chichester, pp 549–576
- Levis S, Foley JA, Brovkin V, Pollard D (1999) On the stability of the high-latitude climate-vegetation system in a coupled atmosphere-biosphere model. *Glob Ecol Biogeogr* 8(6):489–500
- Loveland TR, Reed BC, Brown JF, Ohlen DO, Zhu Z, Yang L, Merchant JW (2000) Development of a global land cover characteristics database and IGBP DISCover from 1 km AVHRR data. *Int Remote Sens* 21:1303–1330
- Lynch-Stieglitz J et al (2007) Atlantic meridional overturning circulation during the last glacial maximum. *Science* 316:66–69
- Madec G, Delecluse P, Imbard M, Lévy C (1998) OPA 8.1 ocean general circulation model reference manual. Rapp Int, LODYC, France, 200 pp
- Marti O, Braconnot P, Dufresne JL, Bellier J, Benshila R, Bony S, Brockmann P, Cadule P, Caubel A, Codron F, De Noblet N, Denvil S, Fairhead L, Fichefet T, Foujols MA, Friedlingstein P, Goosse H, Grandpeix JY, Guilyardi E, Hourdin F, Idelkadi A, Kageyama M, Krinner G, Lévy C, Madec G, Mignot J, Musat I, Swingedouw D, Talandier C (2010) Key features of the IPSL ocean atmosphere model and its sensitivity to atmospheric resolution. *Clim Dyn* 34:1–26
- McManus JF, Francois R, Gherardi J-M, Keigwin LD, Brown-Leger S (2004) Collapse and rapid resumption of Atlantic meridional circulation linked to deglacial climate change. *Nature* 428:834–837
- Milliman JD, Farnsworth KL, Jones PD, Xu KH, Smith LC (2008) Climatic and anthropogenic factors affecting river discharge to the global ocean, 1951–2000. *Glob Planet Change* 62:187–194
- Nobre CA, Sellers PJ, Shukla J (1991) Amazonian deforestation and regional climate change. *J Clim* 4:957–988
- Peltier WR (2004) Global glacial isostasy and the surface of the ice age earth: the ICE-5G (VM2) model and GRACE. *Annu Rev Earth Planet Sci* 32:111–161
- Piao S, Friedlingstein P, Ciais P, de Noblet-Ducoudré N, Labat D, Zaehle S (2007) Changes in climate and land use have a larger direct impact than rising CO₂ on global river runoff trends. *Proc Natl Acad Sci* 104(39):15242–15247
- Pielke RA, Marland G, Betts RA, Chase TN, Eastman JL, Niles JO, Niyogi DDS, Running SW (2002) The influence of land-use change and landscape dynamics on the climate system: relevance to climate-change policy beyond the radiative effect of greenhouse gases. *Philos Trans R Soc Lond A360*:1705–1719
- Piotrowski AM, Goldstein SL, Hemming SR, Fairbanks RG (2005) Temporal relationships of carbon cycling and ocean circulation at glacial boundaries. *Science* 307:1933–1938
- Ramankutty N, Foley JA (1999) Estimating historical changes in global land cover: croplands from 1700 to 1992. *Glob Biogeochem Cycles* 13(4):997–1027
- Ramstein G, Kageyama M, Guiot J, Wu H, Hély C, Krinner G, Brewer S (2007) How cold was Europe at the last glacial maximum? A synthesis of the progress achieved since the first PMIP model-data comparison. *Clim Past* 3:331–339. doi:[10.15194/cp-3-331-2007](https://doi.org/10.15194/cp-3-331-2007)
- Renssen H, Fichefet T, Goosse H (2003) On the non-linear response of the ocean thermohaline circulation to global deforestation. *Geophys Res Lett* 30:1061. doi:[10.1029/2002GL016155](https://doi.org/10.1029/2002GL016155)
- Shaffrey L, Sutton R (2006) Bjerknes compensation and the decadal variability of the energy transports in a coupled climate model. *J Clim* 19:1167–1181
- Sud YC, Walker GK, Kim JH, Liston GE, Sellers PJ, Lau WKM (1996) Biogeophysical consequences of a tropical deforestation scenario: a GCM simulation study. *J Clim* 9(12):3225–3247

- Trenberth KE, Smith L, Qian T, Dai A, Fasullo J (2007) Estimates of the global water budget and its annual cycle using observational and model data. *J Hydrometeorol* 8:758–769
- Valcke S, Declat D, Redler R, Ritzdorf H, Schoenemeyer T, Vogelsang R (2004) The PRISM coupling and I/O system. VECPAR'04. In: Proceedings of the 6th international meeting, vol 1. High performance computing for computational science. Universidad Politecnica de Valencia, Valencia, Spain
- Voldoire A (2006) Quantifying the impact of future land-use changes against increases in GHG concentrations. *Geophys Res Lett* 33:L04701. doi:[10.1029/2005GL024354](https://doi.org/10.1029/2005GL024354)
- Werth D, Avissar R (2004) The regional evapotranspiration of the Amazon. *J Hydrometeorol* 5:100–109
- Winton M (2003) On the climatic impact of ocean circulation. *J Clim* 16:2875–2889
- Wyputta U, McAvaney BJ (2001) Influence of vegetation changes during the last glacial maximum using the BMRC atmospheric general circulation model. *Clim Dyn* 17:923–932